J Bionic Eng 18 (2021) 840–856
DOI: https://doi.org/10.1007/s42235-021-0061-8

Journal of Bionic Engineering
http://www.springer.com/journal/42235

The Unique Strategies of Flight Initiation Adopted by Butterflies on Vertical Surfaces

Huan Shen, Aihong Ji*, Qian Li, Wei Wang, Guodong Qin, Qingfei Han

Institute of Bio-inspired Structure and Surface Engineering, *Nanjing University of Aeronautics and Astronautics*, *Nanjing* 210016, *China*

Abstract

As the basis of flight behavior, the initiation process of insect flight is accompanied by a transition from crawling mode to flight mode, and is clearly important and complex. Insects take flight from a vertical surface, which is more difficult than takeoff from a horizontal plane, but greatly expands the space of activity and provides us with an excellent bionic model. In this study, the entire process of a butterfly alighting from a vertical surface was captured by a high-speed camera system, and the movements of its body and wings were accurately measured for the first time. After analyzing the movement of the center of mass, it was found that before initiation, the acceleration perpendicular to the wall was much greater than the acceleration parallel to the wall, reflecting the positive effects of the legs during the initiation process. However, the angular velocity of the body showed that this process was unstable, and was further destabilized as the flight speed increased. Comparing the angles between the body and the vertical direction before and after leaving the wall, a significant change in body posture was found, evidencing the action of aerodynamic forces on the body. The movement of the wings was further analyzed to obtain the laws of the three Euler angles, thus revealing the locomotory mechanism of the butterfly taking off from the vertical surface.

Keywords: flight initiation, butterfly, vertical surface, body and wing kinematics, speed and stability strategies

1 Introduction

The flight of insects includes important processes such as initiation, hovering flight, fast forward flight, and landing[1,2]. Hover flight and fast forward flight are classic subjects of insect flight research, and their research is relatively sufficient[2–4]. By contrast, fewer studies have been conducted regarding the flight initiation phase of insects. However, this stage is the first maneuver in the whole flight process; therefore, it constitutes the basis of flight and directly affects the quality of the insect's subsequent flight. During a takeoff, insects need to accelerate into the air from stillness, which produces two problems: (1) Generating enough acceleration to enter the air and (2) controlling the body posture to maintain a stable flight[5]. For example, in fruit flies, the changes in the amplitudes of the wings flapping and body posture can be combined into a simple feedback system to control the altitude, speed, and heading[6,7]. Therefore, a closer look at the wing-beat kinematics should reveal how wing motion is adapted to external stimuli, such as those experienced during disturbances. However, relative to hovering or fast forward flight, the instability of insects in the takeoff phase is more obvious, and it is extremely challenging for observation[8].

The current research on the flight initiation process of insects is generally related to taking off from horizontal grounds. Flight initiation strategies can be divided into two types: takeoff by the action of the legs alone, and takeoff by the joint action of wings and legs. Animals that accelerate from the ground using the force of their legs include locusts[9], crickets[10], fruit flies[11], leafhopper insects[12] and birds[13,14]. Pond observed the takeoff process of a locust and indicated that it first jumps into the air with its legs and then begins to flap its wings, from the hindfoot tarsus to the ground to start flapping, and the time interval is usually about 33 ms[9]. And this kind of initiation often occurs during an insect's stimulated escape takeoff. Dickinson and other researchers have found that when flies take off, they first fully jump into the air before opening their wings to start flapping[11,15]. Sun Mao and others observed the rapid takeoff process of bee flies through experiments, and they calculated and analyzed the aerodynamic force

***Corresponding author:** Aihong Ji
E-mail: meeahji@nuaa.edu.cn

during takeoff. Overall, they found that bee flies have the ability to achieve rapid takeoff by increasing the leg force under stimulated conditions[16]. Before an autonomous takeoff, the insects can synergize their wings and legs. First, the flies open their wings toward the back of their back. As the hind legs begin the takeoff, the wings simultaneously flap down quickly and the fly becomes completely airborne[11,16]. Truong *et al*.[17] analyzed the non-jumping takeoff of a rhinoceros beetle, and observed that takeoff occurred at the end of the third wing beat. In a non-jump takeoff process, insects rely more on the aerodynamic force generated by wing flapping than on the force generated by leg actions. This process is slower and more stable than jump takeoff, and the body is not largely rotated.

Unlike takeoff from a horizontal plane, takeoff from a vertical surface is accompanied by substantial changes in an insect's body posture. For instance, the pitch angle is adjusted as the insect transitions from vertical attachment to the wall to a horizontal flight attitude. Meanwhile, the yaw angle changes as the insect alters its orientation from toward the wall to away from the wall. Therefore, takeoff from a vertical surface is not as simple as takeoff from a horizontal surface. As animals that can fly, few birds can attach to vertical walls, let alone takeoff from vertical surfaces. But most insects with flying ability can accomplish this behavior. As a representative of flying insects, the study of butterflies' take-off strategies in the vertical surface provides a reference for other insects' flight research[18,19]. The measurement of its kinematic behavior can also be extended to other organisms. At the same time, this takeoff strategies also laid the foundation for the amphibious research of the Flapping Micro Aerial Vehicle (FMAV).

What unique strategies are employed by a butterfly taking off from a vertical surface? Do the legs play an important role in the flight of butterflies, as observed in many other insects? How do butterflies weigh the relationship between speed and stability throughout the takeoff process? Do wings exert an important influence on the changing body posture? To verify the above conjectures, we observed the takeoff maneuvers of *Tirumala limniace* butterflies. As a typical large-winged flapping insect, the aspect ratio of the wings is relatively small, even less than 1, and the flapping frequency is low. Therefore, the lower flutter frequency and larger wing area provide more convenience for observation. In this study, four high-speed cameras were used for simultaneous shooting to get the kinematic data of the butterfly in the whole process. From their body posture, we could obtain the necessary centroid displacement and Euler angle for figuring out their taking off strategy. Then, through an in-depth study of the wing motions, we revealed the main reasons for the flight attitude control.

2 Materials and methods

2.1 Preparation

In all the experiments, we selected *Tirumala limniace* butterflies taken from a lab colony. After hatching the chrysalis with a temperature of 25 ˚C and a humidity of about 60%, the adults were fed with honey water for four days. We selected 10 individuals for the experiment. After the experiment, the morphological parameters of these 10 samples were measured, and the measurement results are shown in Table 1. According to the morphological measurements of the samples, average-sized wings were chosen for 3D scanning. The separated wings were washed with distilled water and were allowed to dry naturally at room temperature of 20 ˚C – 25 ˚C and 60% humidity. To reduce the impact of surface

Table 1 Morphological and mass parameters of the wing and body

Item	Value
Total mass (m)	234.2 ± 1.3 mg
Wingless weight (m_1)	224.7 ± 0.8 mg
Single wing mass (m_2)	0.0095 ± 0.6 mg
Wingspan (a)	88.18 ± 1.23 mm
Wing characteristic chord length (b)	32.04 ± 0.78 mm
Distance between wings roots (c)	4.66 ± 0.32 mm
Body long axis distance (d)	27.78 ± 0.64 mm

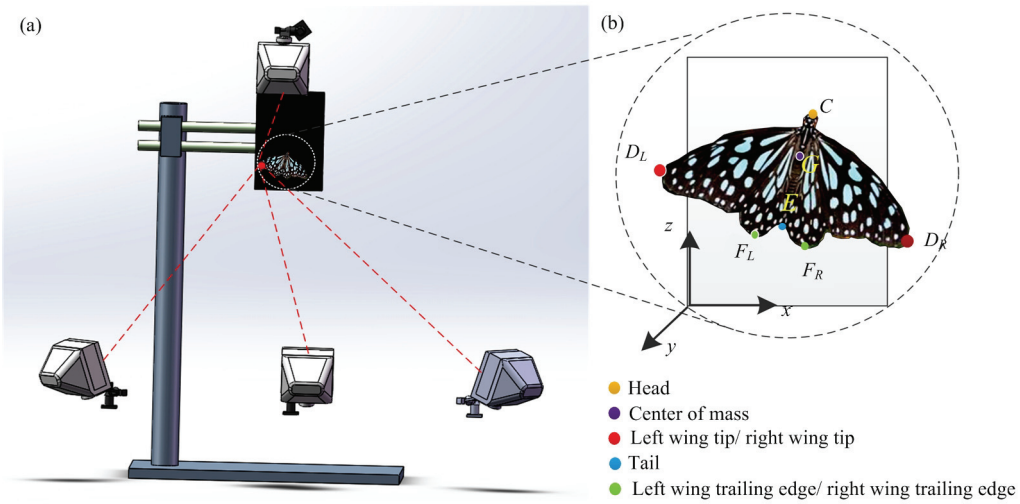

Fig. 1 (a) Setup of the kinematic experiment; (b) illustration of the monitored angles. Four cameras operate simultaneously. After data processing, the absolute coordinates at any time during the entire takeoff process can be obtained. The yellow dot represents the head, the purple dot represents the center of mass, the red dots represent the wing tips, the blue dot represents the butterfly's tail, and the green dots represent the trailing edge. The frame O, x, y, z is fixed on the earth.

reflectivity, color, and curvature characteristics on the laser data, an imaging agent (JIP145, Japan) was sprayed on the surface of the wing to achieve a coloring effect. Because the wing is composed of a free-form surface, the developer was applied as thinly as possible to ensure uniformity of the coating. After the wings were dried, a 3D laser scanner (JTscan-MS-50, China) with ±0.01 mm sensitivity was used for scanning from the dorsal side to the ventral side to obtain the point cloud data of the butterfly wing. The reverse engineering software was used to delete the noise points and simplify the point cloud data, the string deviation method and Gaussian filter were used smooth the point cloud data and complete the reconstruction of the butterfly wings.

2.2 High-speed photogrammetry

To record the entire taking off process of the butterflies from vertical walls, each individual was placed on a rectangular plate perpendicular to the ground. Fig. 1 shows a sample of a butterfly laid on a plate that is 100-mm long and 100-mm wide. The launching platform was surrounded by four high-speed cameras (Prime 17 W, NaturalPoint, Inc., Corvallis, OR, USA), which could provide four different angles of view for the entire taking off process. Each camera was sensitive with infrared light, so there was no need to use additional light supplementary equipment, thus avoiding the impact of the light problems on the experiment. The four cameras adopt a synchronous trigger connection, and the shooting frequency was 360 Hz. After the butterfly steadily stopped at the plane, the shooting switch was triggered to record the entire taking off process from the beginning.

After obtaining the takeoff sequences by the high-speed camera from four angles at the same time, some characteristic points of the butterfly body were manually tracked: head, tail, center of mass (COM) and wings (leading edge, trailing edge). Then, the Direct Linear Transformation (DLT) method (Hedrick lab, University of North Carolina, USA) was used to obtain the coordinates of these feature points at any time of the entire process[20,21].

2.3 Calibration and data processing

To describe the flying speed and trajectory of the butterfly during takeoff, the obtained coordinates by the DLT method were considered as inertial coordinates. The inertial coordinate system is fixed to the earth, and the lower-left corner of the takeoff platform is considered as the flight base point, which is the origin O of the coordinate system. The coordinate axes x_g and y_g are in the horizontal plane, where the axis x_g is parallel to the takeoff plane, and the axis y_g is perpendicular to the x_g axis and points outward. The axis z_g is vertically upward,

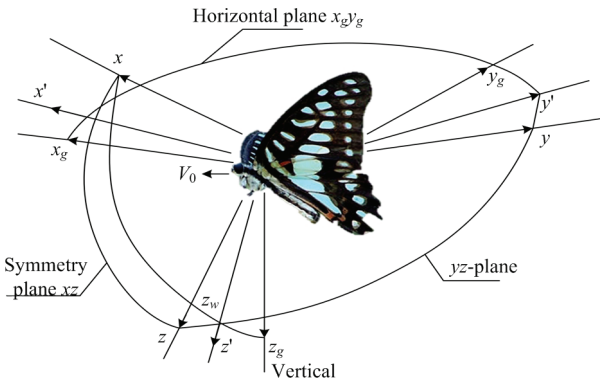

Fig. 2 Definition of the coordinate systems of the flying butterfly, showing the local wing-base-fixed (x',y',z'), local body-based-fixed (x,y,z) and global earth-fixed (x_g, y_g, z_g) coordinate systems. The origin O' of the wing-base-fixed coordinate system lies at the wing base, with the X-axis normal to the stroke plane (the yz plane as defined by Ellington (Liu *et al.*, 1998), the Y-axis vertical to the body axis, and the z-direction parallel to the stroke plane.

as shown in Fig. 1. The left-wing tip coordinates of the butterfly in the inertial reference frame were defined as $D_{\mathrm{L}}(x_{\mathrm{g1}}, y_{\mathrm{g1}}, z_{\mathrm{g1}})$, the right wing tip as $D_{\mathrm{R}}(x_{\mathrm{g2}}, y_{\mathrm{g2}}, z_{\mathrm{g2}})$, the center of mass as $G(x_{\mathrm{g3}}, y_{\mathrm{g3}}, z_{\mathrm{g3}})$, the tail as $E(x_{\mathrm{g4}}, y_{\mathrm{g4}}, z_{\mathrm{g4}})$, the left-wing trailing edge as $F_{\mathrm{L}}(x_{\mathrm{g5}}, y_{\mathrm{g5}}, z_{\mathrm{g5}})$, and the right wing trailing edge as $F_{\mathrm{R}}(x_{\mathrm{g6}}, y_{\mathrm{g6}}, z_{\mathrm{g6}})$. As shown in Fig. 1, the front and rear wings of the butterfly fit closely together, so their movements are basically the same. The front and rear wings on the same side can be regarded as a single wing.

To describe the butterfly attitude, it is necessary to introduce an insect body coordinate system that has the same origin as the inertial coordinate system and changes with the insect's movement posture (Fig. 2). The X axis is parallel to the radial direction of the insect body, the Y axis is perpendicular to the X axis outwards, and the Z axis is perpendicular to the plane composed of the x and y axes. The wings coordinate system was located at the root of the wing (x', y', z'). This is a secondary conversion process. When analyzing the posture and behavior of the butterfly body, only the first transformation was used, and the absolute coordinates obtained by the DLT method were transformed into the body coordinates: Eq. (1). Where c represent cos, s represent sin, $(\theta_{\mathrm{yaw}}, \theta_{\mathrm{pitch}}, \theta_{\mathrm{roll}})$ represents the Euler angle of the conversion between two coordinate systems. After transformation, the coordinates of 6 marker points in the body coordinate system are obtained. Then, to analyze the movement of the wings, another conversion is needed: Eq. (2).

The movement of the insect wings can be divided into three directions:

(1) The flapping motion along the X axis is defined as the flapping angle $\phi(t)$;

(2) The swing motion along the Z axis is defined as the swing angle $\psi(t)$; and

(3) The torsional motion along the Y axis is defined as the twist angle $\omega(t)$.

3 Results

3.1 Locomotion behaviors

Each butterfly was tested 10 times, 5 groups with higher quality were selected. We also observed the asymmetry of the flapping of the wings, where the butterfly did not raise the left and right wings at the same time, and the flapping amplitude was also different. In our 50 digital takeoff experiments, the butterfly simultaneously flapped the left and right wings only four times, and in 30 instances, the butterfly began its movement by raising the left wing first, and in the remaining 16 instances, it began with the right wing. The duration of wing opening (interval from the beginning of the wing movement to the completion of the entire downstroke) was not significantly different between right and left wings (left: 24 ms ± 3 ms, right; 26 ms ±

$$\begin{bmatrix} x_{\mathrm{g}} \\ y_{\mathrm{g}} \\ z_{\mathrm{g}} \end{bmatrix} = \begin{bmatrix} c\theta_{\mathrm{yaw}}c\theta_{\mathrm{roll}} - s\theta_{\mathrm{yaw}}c\theta_{\mathrm{pitch}}c\theta_{\mathrm{roll}} & c\theta_{\mathrm{yaw}}s\theta_{\mathrm{roll}} + s\theta_{\mathrm{yaw}}c\theta_{\mathrm{pitch}}c\theta_{\mathrm{roll}} & s\theta_{\mathrm{yaw}}s\theta_{\mathrm{pitch}} \\ -s\theta_{\mathrm{yaw}}c\theta_{\mathrm{roll}} - c\theta_{\mathrm{yaw}}c\theta_{\mathrm{pitch}}s\theta_{\mathrm{roll}} & -s\theta_{\mathrm{yaw}}s\theta_{\mathrm{roll}}s\theta_{\mathrm{pitch}} + c\theta_{\mathrm{yaw}}c\theta_{\mathrm{pitch}}c\theta_{\mathrm{roll}} & c\theta_{\mathrm{yaw}}s\theta_{\mathrm{pitch}} \\ s\theta_{\mathrm{pitch}}s\theta_{\mathrm{roll}} & s\theta_{\mathrm{roll}}c\theta_{\mathrm{pitch}} & c\theta_{\mathrm{pitch}} \end{bmatrix} \begin{bmatrix} x \\ y \\ z \end{bmatrix}, \tag{1}$$

$$\begin{bmatrix} x \\ y \\ z \end{bmatrix} = \begin{bmatrix} c\phi c\omega - s\phi c\psi c\omega & c\phi s\omega + s\phi c\psi c\omega & s\phi s\psi \\ -s\phi c\omega - c\phi c\psi s\omega & -s\phi s\omega s\psi + c\phi c\psi c\omega & c\phi s\psi \\ s\psi s\omega & s\omega c\psi & c\psi \end{bmatrix} \cdot \begin{bmatrix} x' \\ y' \\ z' \end{bmatrix}. \tag{2}$$

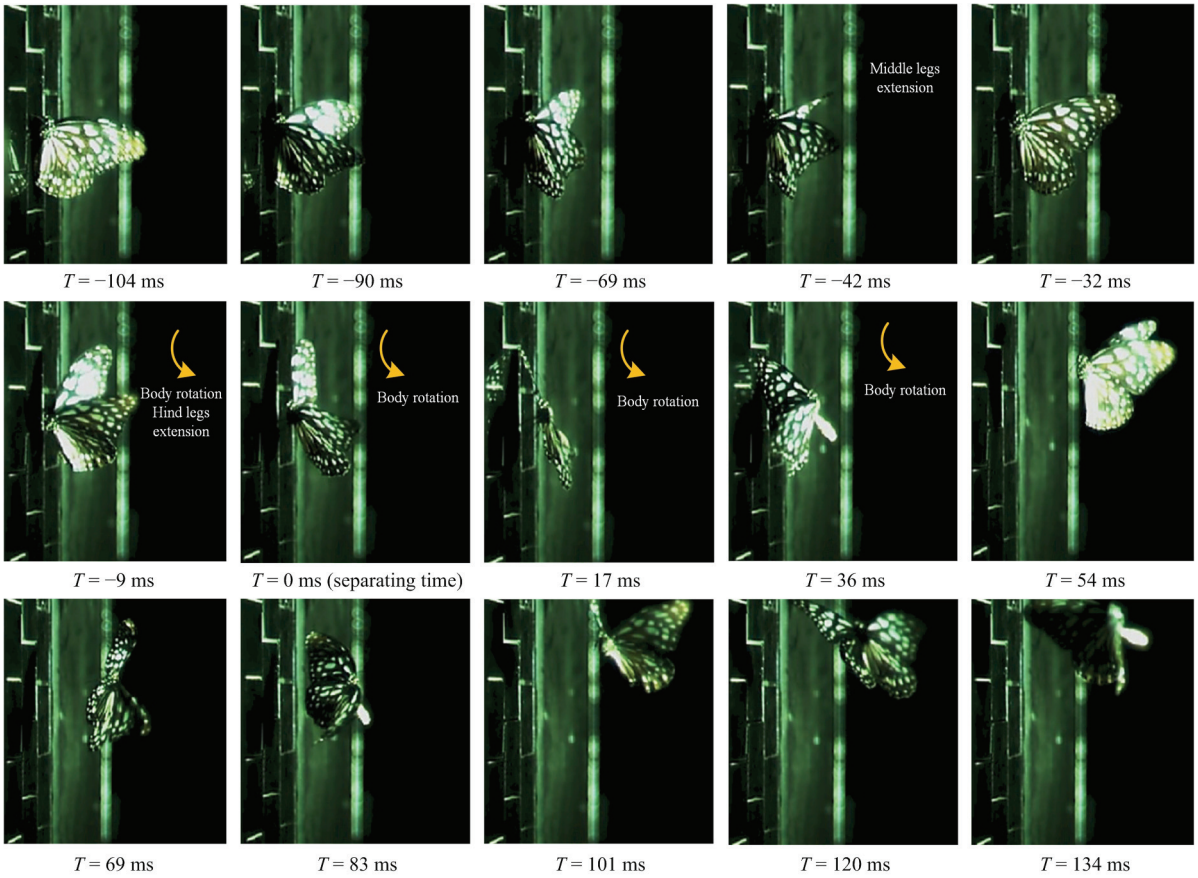

Fig. 3 Video sequences of the butterfly starting flight. (Only one of the four camera views is shown. The times noted are the separation of the body from the wall. The direction of body rotation is marked with a yellow arrow. For the complete video sequences, see the electronic supplementary material, movie 1.)

2 ms; $P = 0.65$, Kruskal-Wallis test). Therefore, we assumed that lifting the left or right wing first is completely random, and only the individuals that first raised the left wing were further analyzed. The key frames were extracted from the experimental video, as shown in Fig. 3.

The whole takeoff process can be divided into three stages. Firstly, the preparation phase, the butterfly basically remained stationary on the takeoff plane, while the wings remained flat. The leading edge of the wing was substantially perpendicular to the trunk axis. Then, the initiation phase, the butterfly's wings start to expand from closed ($t = -106$ ms to $t = -69$ ms). This process is usually not symmetrical, and there are differences in the spread of the left and right wings. Of course, due to the limitation of the vertical wall, the flapping amplitude of the butterfly wing is small at this moment. During the upstroke of the first cycle, the middle leg began to extend ($t = -42$ ms), gradually lifting the body. Due to the asymmetry of the first flutter, during the second cycle, the body has a turning process, and at the same time, the hind legs were lifted ($t = -9$ ms). The butterfly gradually leaves the wall under the combined action of its wings and legs. During this process, the middle legs begin to rise during the upstroke phase, and the extension of the hind legs continues until the body leaves the wall (as shown in Fig. 4).

Finally, the disengagement phase, after leaving the wall, the butterfly would drop a short distance due to the insufficient lift in order to maintain its gravity ($t = 0$ ms to $t = 36$ ms). At the same time, the frequency of flutter has increased (see Fig. 5). Subsequently, with the increase in the flapping amplitude in the next few flutters, the produced air reaction force allowed it to maintain its position in the air, and it then gradually moved away from the wall ($t = 54$ ms). After completely leaving the

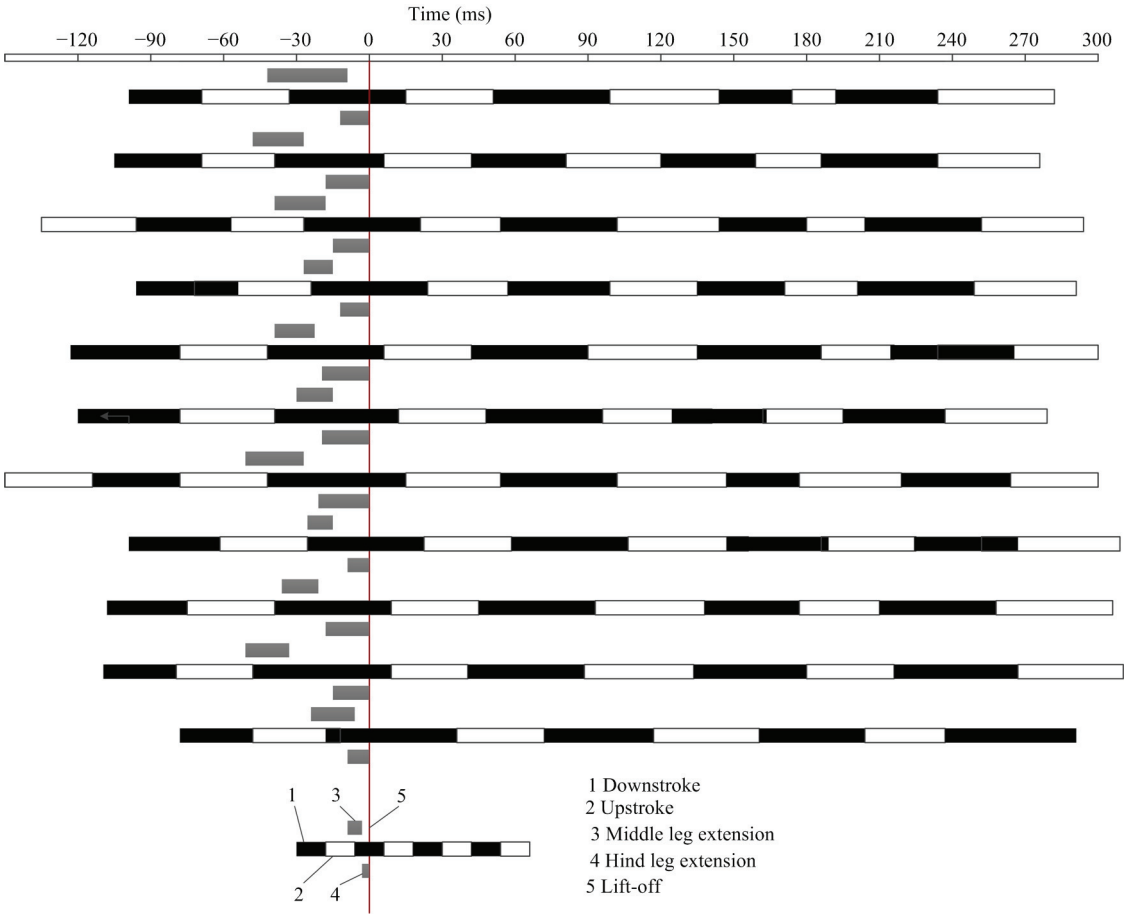

Fig. 4 Timelines of take-off events ($N = 11$). Each timeline represents an event sequence for an individual butterfly. The black and white bands represent the duration of the down stroke and the upstroke respectively, the grey bands represent the duration of the middle leg and hind leg extension.

wall, the flapping angle of each wing was greater than 90 degrees, but the flutter of the left and right wings was still not completely symmetrical, so the deviation of the amplitude and phase between the two wings led to yaw and roll torques. Thus, the butterfly gradually changed its direction (t = 101 ms). Later, the flapping frequency decreased a little bit and stabilized, and the butterfly gradually moved away from the wall (t = 120 ms). During the entire takeoff process, the butterfly always kept the line from the leading edge to the wing root perpendicular to the body axis so as to maintain its wingspan at a maximum value, which also makes it easier to calculate the wing Euler angle.

3.2 Changes in the body posture during the flight initiation

The relationship between the displacement of the center of mass and time of the individuals that raised the left wing first was plotted, as shown in Fig. 5a (30 trials for 10 individuals). It can be seen that the displacement of the butterfly in the X direction was much smaller than in the other two directions (Y, Z), reflecting the relatively small movement of the butterfly in the lateral direction. This shows that the butterfly tries to minimize unnecessary movements during takeoff and that its main purpose is to keep away from the wall. The Euler angle of the butterfly body was plotted, and the maximum, minimum, and average three posture angle changes were counted. Fig. 6d shows the statistics of the maximum, minimum, and average three posture Euler angles of the butterfly. It can be seen that the maximum value of the butterfly yaw angle (60.34° ± 15.65°) is much larger than that of the other two angles, while not much differences were found between the pitch and roll angles.

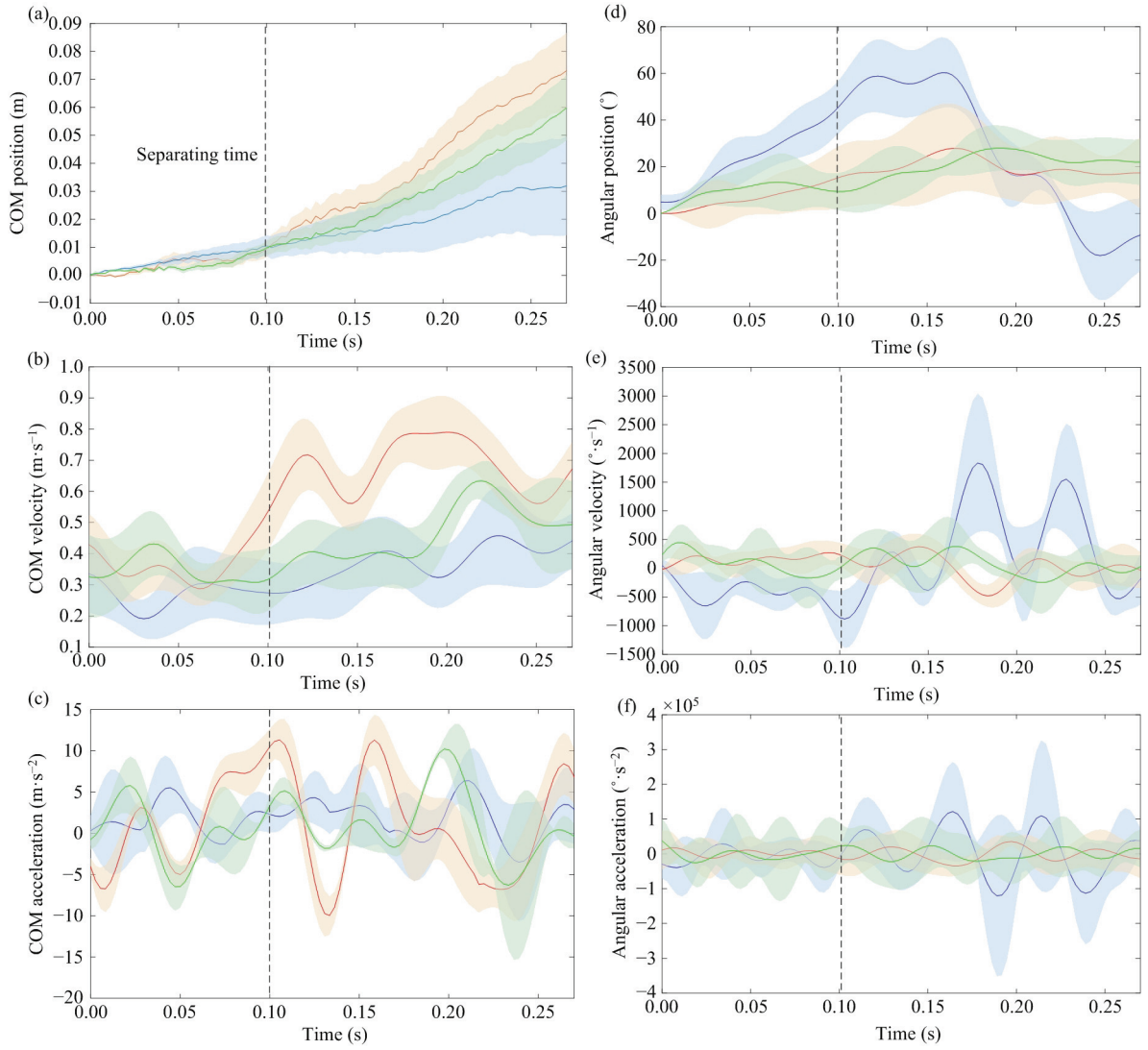

Fig. 5 Average time courses for the (a) (b) (c) translational and (d) (e) (f) rotational kinematic variables. (In (a) (b) (c), the blue lines are the mean values for the *X*-direction, the red lines are the mean values for the *Y*-direction, and the green lines are the mean values for the *Z*-direction. In (d) (e) (f), the blue lines are the mean values for the yaw angle, the red lines are the mean values for the pitch angle, and the green lines are the mean values for the roll angle. The shaded area around the mean shows the standard error. The roll and yaw values for the position, velocity, and acceleration have been adjusted as if all the first rolling and yawing motions were to the butterfly's right.)

This shows that the butterfly's adjustment of the flight direction during takeoff mainly relies on adjusting the yaw angle. The changes in the pitch and roll angles can also adjust the attitude of the butterfly and thus affect the flight direction; however, their impact is not as significant as that of the yaw angle.

By comparing the COM speed in the three directions, as shown in Fig. 5b, it can be seen that the speed of the butterfly at the separation point in the *X*-axis, *Y*-axis, and *Z*-axis directions was $v_{x_1} = 0.27\ \text{m·s}^{-1} \pm 0.10\ \text{m·s}^{-1}$, $v_{y_1} = 0.54\ \text{m·s}^{-1} \pm 0.12\ \text{m·s}^{-1}$, and $v_{z_1} = 0.32\ \text{m·s}^{-1} \pm 0.10\ \text{m·s}^{-1}$. Also, the speed on the initiation plane was $v_{\perp} = \sqrt{v_x + v_y}$, $\arctan(v_{\perp} / v_y) \approx 51.98°$. The maximum speeds in the three directions were $v_{x_1} = 0.46\ \text{m·s}^{-1} \pm 0.16\ \text{m·s}^{-1}$, $v_{y_1} = 0.79\ \text{m·s}^{-1} \pm 0.11\ \text{m·s}^{-1}$, and $v_{z_1} = 0.63\ \text{m·s}^{-1} \pm 0.06\ \text{m·s}^{-1}$. This shows that the moving tendency of the butterfly in the *Y*-axis and *Z*-axis directions is still greater than that in the *X*-axis (lateral) direction.

The acceleration curves in the *X*-axis, *Y*-axis, and *Z*-axis directions are shown in Fig. 5c. It can be seen that the acceleration in the three directions at the separation point was $a_{x_1} = 2.50\ \text{m·s}^{-2} \pm 2.31\ \text{m·s}^{-2}$, $a_{y_1} =$

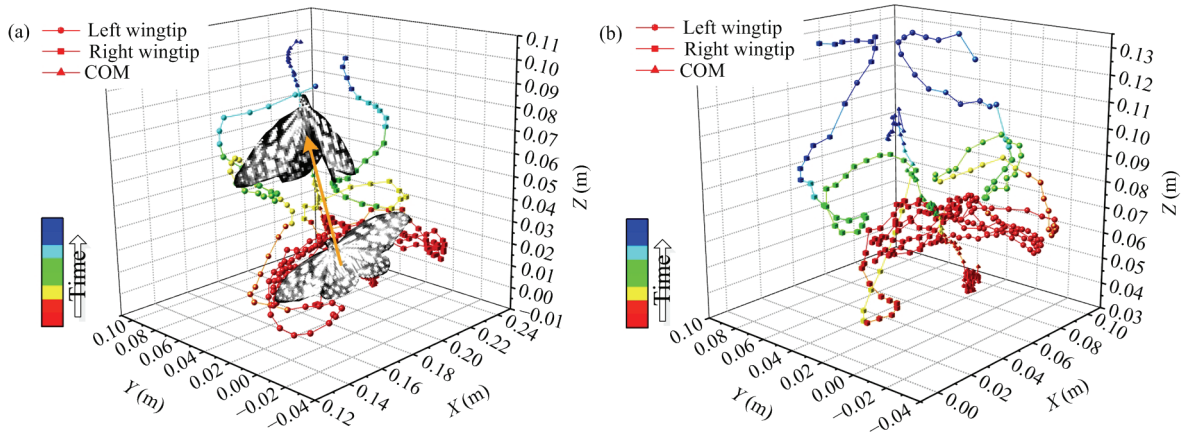

Fig. 6 Trajectory curves of the center of mass and the left/right wing tip of the butterfly during its wing-flapping motion (two typical processes). The red-to-blue gradient indicates the order of the butterfly takeoff. Cubes and balls respectively indicate the movements of the left and right wing tips, and tetrahedrons indicate the displacement of the butterfly's center of mass (COM).

9.61 $m \cdot s^{-2} \pm 2.35$ $m \cdot s^{-2}$, and $a_{z_1} = 2.20$ $m \cdot s^{-2} \pm 0.65$ $m \cdot s^{-2}$, which shows that the butterfly exerted more force in the direction perpendicular to the takeoff plane. The maximum reached acceleration after takeoff was $a_{x_2} = 6.33$ $m \cdot s^{-2} \pm 3.06$ $m \cdot s^{-2}$, $a_{y_2} = 11.30$ $m \cdot s^{-2} \pm 2.54$ $m \cdot s^{-2}$, and $a_{z_2} = 10.21$ $m \cdot s^{-2} \pm 1.25$ $m \cdot s^{-2}$, so the acceleration in the *Y*-axis direction was essentially equal to the acceleration in the *Z*-axis direction and larger than that in the *X*-axis direction.

Based on the angular velocity curve of the butterfly attitude angle, as shown in Fig. 5e, the maximum angular velocity of the yaw angle was 1834.29 $^\circ \cdot s^{-1} \pm 1205.85$ $^\circ \cdot s^{-1}$, the maximum elevation angle was -480.45 $^\circ \cdot s^{-1} \pm 193.78$ $^\circ \cdot s^{-1}$, and the maximum roll angle was 449.40 $^\circ \cdot s^{-1} \pm 294.17$ $^\circ \cdot s^{-1}$. The maximum value of the yaw angle was much larger than that of the other two, which shows that the butterfly produced a positive roll action during takeoff. We defined a relative steadiness metric *S* that is a linear transformation of the butterfly's angular speed[16]:

$$S = 1 - \|\varphi\| / \|\varphi\|_{\max}, \quad (3)$$

where $\|\varphi\|$ is the vector sum of the angular velocity about all the three body axes, and $\|\varphi\|_{\max}$ is the largest angular speed observed in our experiments, 1893.97 $^\circ \cdot s^{-1}$. When $S = 1$, the butterfly flight was in a stable state with an angular speed of 0 $^\circ \cdot s^{-1}$. The butterfly flight was more unstable with the smaller values of *S*.

3.3 Changes in the butterfly attitude angle during takeoff

To quantitatively describe the wings movement, the wing tip trajectory needed to be obtained. In the experiment, we tracked and captured the changes in the wing tip and the center of mass during initiation. Connected with a line, the wings trajectory can intuitively be observed. As shown in Fig. 6, it can be seen that the *X*-*Z* plane is the initiation plane, as the butterfly took off from the lower right corner of the image and moved toward the upper left corner. By comparing the left and right wingtip trajectories, we could find that their amplitudes are quite different. This is closely related to the instability of the butterfly takeoff process.

Through the conversion and calculation of the motion coordinate system, the flapping angle $\phi(t)$, twist angle $\psi(t)$, and swing angle $\omega(t)$ during takeoff could be obtained, respectively. Low-pass filtering was performed on the original data using fast Fourier transform with a cutoff frequency of 45 Hz. Fig. 7 shows the Euler angles of the left and right wings.

Unlike the situation in which the butterfly was in a stable flight state, the Euler angles of the wing greatly changed during initiation. We defined a cycle for the wings from overlapped to unfolded, and then overlapped after the downstroke and upstroke. It can be deduced that the butterfly completed the initiation process in 2 – 3 cycles. As shown in Fig. 7a, by comparing the phases of the three Euler angles, it can be deduced that the phase

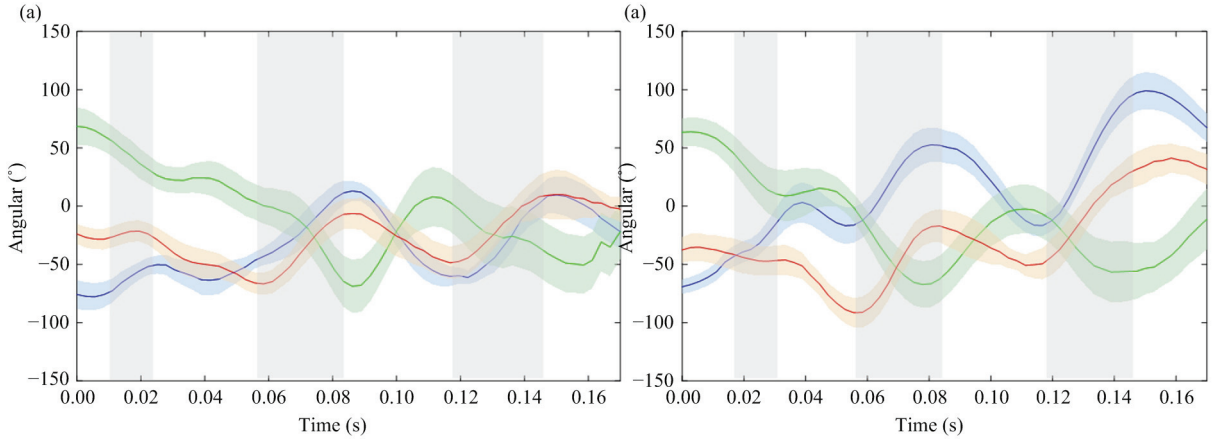

Fig. 7 Time histories of the average wing-flapping motion. (The blue lines are the mean values for the flapping angle, the green lines are the mean values for the torsion angle, and the red lines are the mean values for the swing angle. The shaded area around the mean values shows the standard error, the gray bars represent the upstroke.)

difference between the $\phi(t)$ and $\omega(t)$ was small and that the maximum difference was only 0.009 s. However, the phase in $\psi(t)$ was basically half a cycle from the other two angles.

After comparing the Euler angles of the left and right wings, respectively, as shown in Fig. 8, it can be found that at the beginning of the takeoff phase, the phases of $\phi(t)$ and $\omega(t)$ for the left and right wings were not exactly the same. However, at the later stage of the takeoff phase, the phases of the two wings were gradually consistent. At the beginning of the takeoff phase, the amplitudes of $\phi(t)$ and $\omega(t)$ were small. As the butterfly left the plane, the amplitudes of the two angles significantly increased, but the amplitudes of $\psi(t)$ decreased. Moreover, the change range of the Euler angle of the left and right wings was also different. This is particularly evident in the flapping angle. The amplitude of the right wing was significantly larger than that of the left wing.

Having analyzed the curve of the wing's motion parameters with time, the Fourier series were chosen to describe it. A fitting function of order 4 or higher is considered to ensure the accuracy and the following equation is obtained:

$$\phi_{\mathrm{L,R}}(t)=\sum_{n=0}^{n=6}[\phi_{\mathrm{cn}}\cos(nkt)+\phi_{\mathrm{sn}}\sin(nkt)], \tag{4}$$

$$\psi_{\mathrm{L,R}}(t)=\sum_{n=0}^{n=6}[\psi_{\mathrm{cn}}\cos(nkt)+\psi_{\mathrm{sn}}\sin(nkt)], \tag{5}$$

$$\omega_{\mathrm{L,R}}(t)=\sum_{n=0}^{n=6}[\omega_{\mathrm{cn}}\cos(nkt)+\omega_{\mathrm{sn}}\sin(nkt)], \tag{6}$$

$$K=\frac{2\pi fc}{2U}, \tag{7}$$

$$U=2\theta Rf, \tag{8}$$

where K represents the attenuation frequency, f represents the flapping frequency, c represents the chord length of the wing, U represents the relative speed of the wing tip, θ represents the flapping amplitude of the wings. ϕ_{cn}, ϕ_{sn}, ψ_{cn}, ψ_{sn}, ω_{cn} and ω_{sn} were obtained by solving a matrix equation. Through the above equation, the wing's motion state can be completely determined. Also we can get the changes of the average stroke angle $\bar{\Phi}$ and the stroke amplitude angle Φ during takeoff. They are defined by $\Phi=(\theta_{\max}-\theta_{\min})$ and $\bar{\Phi}=(\theta_{\max}+\theta_{\min})/2$, where $\theta_{\max}$ and $\theta_{\min}$ are the maximum and minimum values of the Engle angle, respectively.

3.4 Aerodynamics of butterfly wings during takeoff

In this chapter, the reconstructed butterfly wing model is moved with the motion function (Eqs. (4) – (6)), and the velocity vectors on the flapping plane and the absolute iso-vorticity surfaces around the butterfly wing (as shown in Fig. 9) are obtained. The influence of the flow field around the butterfly wings is comprehensively considered combining the two-dimensional and

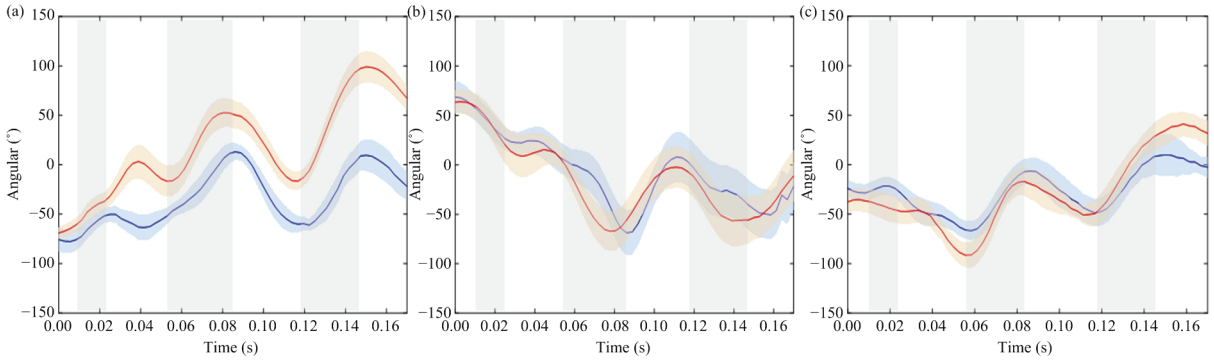

Fig. 8 Time histories of the average wing-flapping motion (The blue lines are the mean values for the left wing, and the red lines are the mean values for the right wing. The shaded area around the mean shows the standard error, and the gray bars represent the upstroke.)

three-dimensional flow conditions on the take-off process.

As shown in Fig. 9a, the butterfly wing is at the beginning of the upstroke, and ring-shaped vortex structures which are produced by the last downstroke appear near the upper wing surfaces of the left and right wings respectively. Due to the asymmetric flapping of the left and right wings, the starting vortex generated is asymmetrical, and the degree of Trailing-Edge Vortex (TEV) separation near the right wing is significantly higher than the left wing. Also, since the starting vortex balances the circulation of the bound vortex, the air in the vortex ring produces a downward impulse, forming a low pressure area. Due to the Wagner effect, the half-period starting vortex and stopping vortex have the same meaning, the lift cycle is generated, and the lift gradually increases[22].

In the upstroke process, as shown in Fig. 9b, the flapping velocity of both left and right wing gradually increases, and the phase tends to be symmetrical. The vortex ring generated by the last downstroke gradually becomes weaken, and a horseshoe-shaped vortex including a Leading Edge Vortex (LEV), a wingtip vortex (TV) and a TEV appears near the lower wing surface again[23]. With the flapping process of the wing, the size of LEV and TEV gradually increases, as shown in Figs. 9c and 9d. Meanwhile, the LEV gradually moves towards the wing tip, and the intensity of TV gradually increases. As the upstroke angle increased, the LEV is limited to a narrow area near the wing tip, consequently, the lift decreased beyond the peak, while TV and TEV gradually expand to the tailing edge. At the mid-upstroke, the ring-shaped vortex generated by the last flapping gradually detaches. However, the velocity of the wing gradually decreased, increasing the pressure at the lower surface of the wing plane and slowing the lift decline. Despite the low wing speed, the lift was maintained by coupling of the non-stationary vortices, skipping the gradual rise and fall of lift caused by the Wagner effect.

Fig. 9e shows the transition of wings from upstroke to downstroke. Among them, the butterfly wings experienced a complete overlap to open. As the gap between the two wings increased rapidly, a large amount of air flow poured in. The LEV and the TEV appear from the wing root to the leading edge and the trailing edge respectively, whose directions are from the lower surface of the wing to the upper surface. A ring-shaped vortex is gradually formed on the edge of the butterfly wing. However, due to the close distance between the two wings, the ring-shaped vortex structure is seriously coupled in the first half of the downstroke.

As shown in Figs. 9f and 9g, the structure of the ring-shaped vortex produced during the downstroke resembles the wake during the upstroke, but the scale is larger than that. When the wing reaches the horizontal position, the spiral vortex formed by the LEV and TV reaches the maximum scale. This unstable vortex maintains stability so that excessively large unsteady vortices will not be fall off from the wing surface. The coupling effect of the unsteady vortex on the left and right wings also leads to the formation of a negative pressure zone on the upper surface, which helps the butterfly to produce high lift during the downstroke.

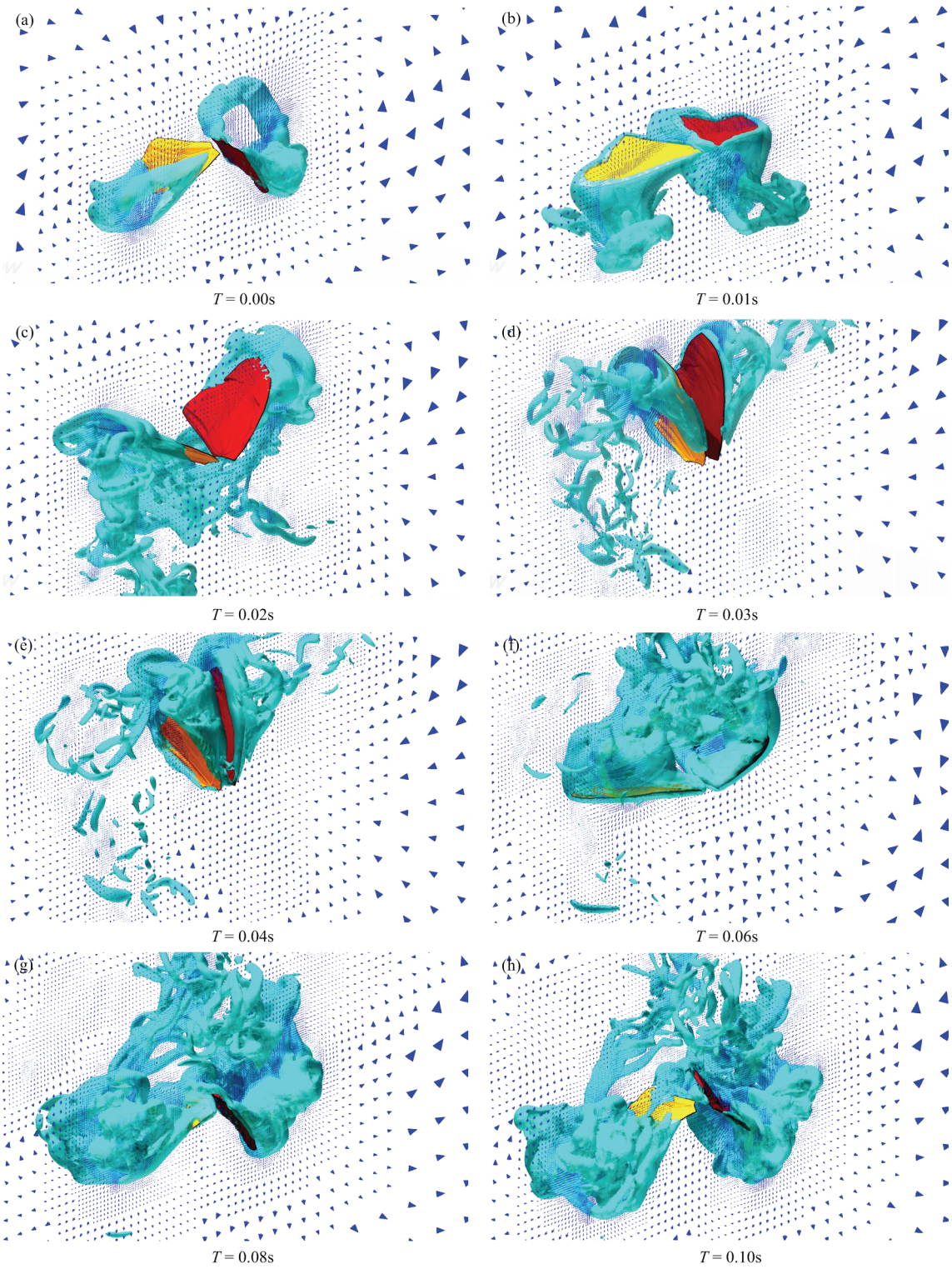

Fig. 9 The flow structures around the butterfly wing during takeoff (velocity vectors and absolute iso-vorticity surfaces).

As shown in Fig. 9h, the butterfly has completed one cycle flapping, and enters the next period process. The LEV appeared in the downstroke gradually breaks and transforms from a 2D structure to a 3D structure. The TV gradually became unstable. The ring-shaped vortex formed with the TEV gradually developed to the

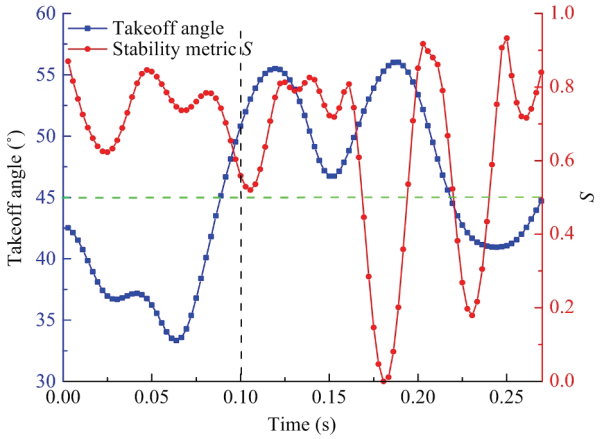

Fig. 10 Takeoff angle and Steadiness metric *S* during initiation. The black dotted line is the dividing point where the butterfly leaves the vertical surface. The green dotted line is the general takeoff angle of an insect from a horizontal plane.

tailing edge and finally separated from the wing surface.

4 Discussion

As there is very little research on insect takeoff from vertical surfaces, the observed process will be compared with insect takeoff from horizontal surfaces. The butterfly altered its posture, and the movements of its wings and legs were intuitively revealed during takeoff. From previous studies, it is known that butterflies cannot complete the takeoff process through wing-flapping or leg actions alone[24]. Therefore, butterfly flight must be initiated through synergy of the legs and wings. By analyzing the kinematics of the center of mass and changes in posture angle of the body, we quantified the relationship between the speed and stability of the flight. Finally, we refined the kinematics of the wings and studied the effects of asymmetric flapping on the butterfly's flight performance.

4.1 The initiation posture on the vertical surface

Four high-speed cameras simultaneously tracked the butterfly's takeoff process on the vertical wall, and the movement sequence of the butterfly's wings and legs could be clearly observed. For most of the individuals, the butterfly first raised its wings to flutter when taking off. After completing a complete cycle, the legs were stretched to raise the trunk. Then with the second cycle of the wings, the four supporting legs left the wall in turn.

This takeoff strategy is relatively common in winged insect initiation. For example, the fruit fly *Drosophila melanogaster*, which has voluntary flight initiations, has at least two different stages of flight initiation: Wing raising and subsequently leg extension[25]. In a study concerning the flight initiation of other butterflies, such as the cabbage butterfly *Pieris rapae*, they also completed the wings lifting first. Then, the hind and middle legs extended in sequence with the body to begin moving upwards, and the wing downstroke occurred much later[24]. It should be noted that the leg strength of the butterfly is not strong, and it is basically impossible to complete the initiation process by solely depending on the action of the legs, such as in the case with the planthopper *Proutista moesta*[26] or the locusta *Schistocerca gregaria*[9]. The takeoff process of the butterfly is a combination of the actions of the leg and the wings.

4.2 Body kinematics

After comparing the speed of the butterfly in the *x*, *y*, and *z* directions, the takeoff angle at the separating point can be calculated to analyze the moment direction. The smaller the angle, the closer to the surface, otherwise, the greater the trend is away from the surface. The takeoff angle is defined by the ratio of the speed perpendicular to the surface to the speed parallel to the surface during the initiation of the butterfly. The speed of the whole process is analyzed, then the curve of the takeoff angle with time is made, as shown in the Fig. 10.

It can be found that the butterfly's takeoff angle reached 51.98° at the separation point, while insects taking off from the horizontal plane have a takeoff angle close to 45°. This reflects that the butterfly has a greater speed in the vertical surface direction during the takeoff process, which could be inferred that the force perpendicular to the surface is greater during the initiation process. After leaving the surface (t = 0.1s – 0.2s), the direction angle fluctuates between 45° – 55°. The velocity in the vertical direction is still greater than in the horizontal direction. This reflects that the butterfly still has an obvious tendency to stay away from the wall. After the flight state gradually stabilizes (t > 0.2s), the angle with the horizontal plane is about 45°, which maximizes the horizontal distance such as in the case

with flies[14,27].

As for the acceleration of the center of mass, for the separation point, the acceleration in the y direction is much greater than that in the other two directions. Namely, the acting force perpendicular to the wall surface is more significant than the other forces. For insects such as *P. rapae*, which have more developed leg muscles, revealing the leg force values close to the eight times reported for locusts during jumping maneuvers[9,28]. For birds, such as the pigeon *Columbia livia*, the hindlimbs have proven to contribute up to 25% of the total velocity during takeoff[27], 93% with the finch, and 95% with the dove[29]. Therefore, it can be concluded that a large part of this perpendicular force to the wall surface is generated by the reaction force of the legs against the wall surface.

By comparing the takeoff speeds of butterflies and planthoppers, we could find that the butterfly takeoff speed is greater than that of the rice planthopper only with wings and less than that with legs. This also indirectly proves that butterfly initiation is a process of wings and legs acting together. By comparing the accelerations of the butterfly and other insects, we could find that the acceleration of the butterfly is only 1/4 and 1/7 of that of the fruit fly in the vertical and horizontal directions, respectively. The takeoff time of fruit flies is also much shorter than that of butterflies. It takes only about 30 ms for a fruit fly to complete an entire takeoff process, while the butterfly takes about 270 ms.

As for the Euler angle of the butterfly body, it can be found that the yaw angle of the butterfly most drastic changes during takeoff. Moreover, after a statistical analysis of the angle change, it can be found that there is a coupling relationship between the three Euler angles change, which is related to the complexity of the butterfly takeoff process. This is common with the flight of the dragonfly, where the three Euler angles of the maneuver flight are changed to varying degrees. While flying forward, only the pitch angle significantly changed[30]. When analyzing the angular velocity of the butterfly, the stability metric S was introduced. Plotting the trend graph of stability S over time, it can be found that as time increases, the fluctuation of stability gradually increases (Fig. 10). In the preparation phase (t = 0 s – 0.1 s), S fluctuates around 0.6 – 0.8. After takeoff, the stability decreased, which was manifested as the increase in the fluctuation of S. At t = 0.18 s, the angular velocity of flight reaches the extreme value and the stability is minimized. But after that, the stability still fluctuates sharply between 0.2 – 1.0. This reflects that the butterfly's initiation in the vertical plane is an unstable process, and the stability further decreases with time. By comparing the initiation process of fruit flies and butterflies, we could find that the butterfly's state at initiation is between the fruit flies voluntary initiation (S = 0.86) and escaping (S = 0.55). After leaving the ground, the angular velocity reaches its peak value, and the stability further decreases[31].

4.3 Wing kinematics

After calculating the Euler angle of butterfly wings, it was found that the phases of the flapping angle and swing angle are basically the same, which are 180 degrees different from the twist angle. This is also very common in other flying insects, such as droneflies[32] and bamboo weevils[33].

By comparing the Euler angles of the left and right wings, we could find a difference in the phase and amplitude, so the changes on both sides were not consistent. By listing the Φ in four cycles, as shown in Table 2, you can find that the amplitude of $\phi(t)$ gradually increases with time, from 13.13° (left) and 19.95° (right) to 70.72° (left) and 115.67° (right). The initial amplitude of $\psi(t)$ is close to that of $\phi(t)$, but after increasing to about 90°, it begins to gradually decrease, and it then finally decreases to about 55° (58.57° (left) and 54.16° (right)). The $\omega(t)$ belongs to a steady rise process whose amplitude increase is relatively small (45.29° (left) and 45.26° (right) to 58.68° (left) and 92.03° (right)).

The change trend of the $\bar{\Phi}$ is more obvious (Table 3): the average position of the flapping angle and the swing angle both have a clear upward trend, and the mean stroke angle of $\phi(t)$ is respectively −56.97° (left) and −6.7° (right), ascending to −25.82° (left) and 41.20° (right). The $\omega(t)$ from −44.02° (left) and −68.79 (right) up to −19.30° (left) and −4.75° (right). The mean stroke angle of $\psi(t)$ has a downward trend from 23.24° (left) and 12.10° (right) to −21.34° (left) and −29.45° (right).

We could also obtain the asymmetry of the left and right flapping from the Φ and $\bar{\Phi}$, and it was found that

Table 2 Stroke amplitude of the Euler angle

Stroke amplitude(°)	$\phi_L(t)$	$\phi_R(t)$	$\psi_L(t)$	$\psi_R(t)$	$\omega_L(t)$	$\omega_R(t)$
Period 1	13.14 (7.75)	19.95 (7.18)	2.14 (11.05)	6.62 (12.28)	45.28 (9.12)	45.26 (9.94)
Period 2	76.63 (13.19)	69.43 (13.96)	93.12 (15.74)	82.58 (14.26)	60.28 (9.42)	74.52 (11.99)
Period 3	74.27 (8.58)	69.34 (9.18)	76.75 (19.62)	64.80 (17.70)	42.25 (13.15)	33.86 (7.95)
Period 4	70.72 (5.94)	115.67 (15.82)	58.57 (21.10)	54.16 (20.83)	58.68 (16.24)	92.03 (12.43)

Table 3 Mean stroke angle of the Euler angle

Mean stroke angle (°)	$\phi_L(t)$	$\phi_R(t)$	$\psi_L(t)$	$\psi_R(t)$	$\omega_L(t)$	$\omega_R(t)$
Period 1	−56.97 (9.62)	−6.74 (11.07)	23.25 (11.45)	12.10 (14.29)	−44.03 (8.69)	−68.79 (11.13)
Period 2	−25.22 (12.82)	17.99 (13.33)	−22.24 (14.85)	−25.88 (12.94)	−36.53 (9.15)	−54.16 (12.59)
Period 3	−24.05 (13.24)	18.04 (12.35)	−30.43 (17.89)	−34.77 (16.11)	−27.52 (12.86)	−33.83 (13.21)
Period 4	−25.82 (7.87)	41.20 (13.61)	−21.34 (22.87)	−29.45 (21.07)	−19.30 (9.23)	−4.75 (12.24)

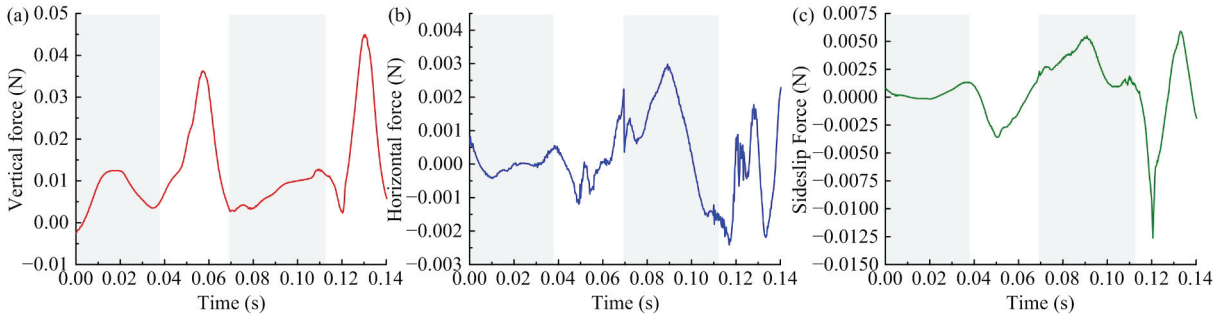

Fig. 11 Time courses of the vertical (lift; a), the horizontal (drag and thrust; b) and sideslip (c) forces over two flapping cycle, the gray bars represent the upstroke

butterflies usually generate an unbalanced force that leads to a significant roll after takeoff. The asymmetry of the wings also takes place in the initiation of the fruit flies. Of the 16 individuals that Dickson conducted the experiments with, only three wings were raised at the same time, while eight raised the left wing first, and the other five raised the right wing first. Alexander also found that when the dragonfly makes a turn, the flapping angle of the left wing is about 40 degrees and that of the right wing is only 10 – 20 degrees[34].

Sun Mao observed the takeoff of a dronefly and found that its mean stroke angle remained essentially the same[35]. The phase of the Euler angles on the left and right wings was also basically the same. Moreover, the dronefly experienced 10 – 14 cycles from the beginning of flapping its wings to takeoff, and its takeoff acceleration (4 $m \cdot s^{-2}$) was also smaller than that of the butterfly (14.77 $m \cdot s^{-2}$). Therefore, the takeoff process should be more stable. The initiation speed and stability always form a pair of opposing physical quantities. When learning and imitating the takeoff strategy of insects, we need to weigh the two quantities to obtain the best takeoff method.

4.4 The mechanism of the flow field during takeoff

The CFD analysis of the butterfly wing shows that a relatively stable vortex structure will be formed on the surface of the butterfly wing when upstroke and downstroke. The staying of the LEV on the wing surface is an important mechanism for the butterfly's lift. This unsteady lift mechanism makes the vertical force basically positive throughout the flapping cycle (Fig. 11a). The reason why the LEV maintains stability may be related to the axial flow caused by the pressure gradient at the core of the LEV[36–39]. To verify this hypothesis, Fig. 12 shows the pressure gradient contours on the surface of the butterfly wing at the mid-upstroke. It can be observed that there is a significant pressure distribution on the wing surface, which is likely to cause the vorticity transport on the wing surface to maintain the stability of

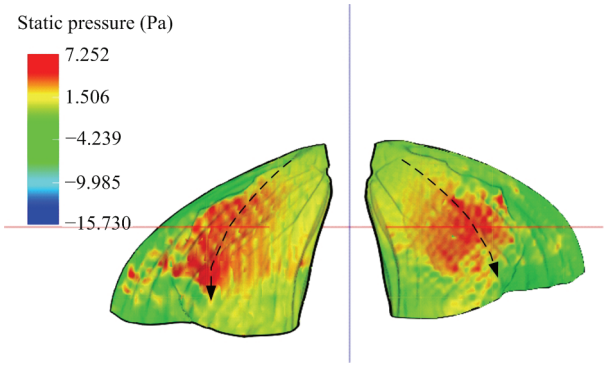

Fig. 12 Pressure gradient contours on the wings of a butterfly at mid-upstroke. The black arrows represent the core and direction of the spanwise pressure gradient on the wing surfaces.

the LEV. Of course, by simulating the entire flapping cycle of the butterfly, it can be found that the LEV will break down in the middle and late stages of the upstroke and downstroke, then a new vortex will be generated, which also leads to the fall back of the lift.

Meanwhile, due to the formation of the Clapping fling mechanism, there is a coupling phenomenon between the left and right wings, which greatly improves the air flow on the upper surface. A large area of low pressure appears in the first half of the downstroke, which results in a higher lift peak at the downstroke than at the upstroke. For hawkmoths and hummingbirds[38–40], downstroke is also the main source of lift (hawkmoth: 30% – 40% for upstroke, 60% – 70% for downstroke; hummingbird: 25% for upstroke, 75% for downstroke). However, for fruit flies[41], the lift force generated in the upstroke is greater for the LEV does not break during the whole flapping cycle.

In the previous section, we have found that the movement of the left and right wings of the butterfly during the takeoff process is asymmetric. This asymmetry causes its body to turn during takeoff. As shown in Fig. 11c, the sideslip force curve is integrated and averaged. It is found that the average sideslip force during takeoff is 0.004 N, indicating the overall direction is to the right, which is consistent with the actual situation. In addition, comparing the horizontal force and the sideslip force (Figs. 11b and 11c), it can be found that the trends of the two curves are similar, which shows that the asymmetric flapping of the left and right wings not only affects the changes in the sideslip force, but also affects the changes in the thrust and drag. Therefore, the asymmetric flapping of the butterfly wings produces two effects: One is to change the direction of movement, and the other is to accelerate away from the vertical surface.

5 Conclusion

Insect flight is an efficient movement, and is widely mimicked in the design of micro-aircraft. Flight initiation from a vertical surface can undoubtedly expand the working space and application range of aircraft. However, this unique movement mode of insects has been little investigated, and our knowledge is very limited. This article carefully observed and quantified the butterfly's takeoff behavior from a vertical surface. The accurately obtained kinematics data will provide valuable experience for future study of insect takeoff strategies. These unique strategies can be also promoted and applied to amphibious FMAV, which can help achieve the purpose of taking off from vertical walls and entering the air more stably and quickly.

Acknowledgment

This work was supported by the National Key R&D program of China (grant no. 2019YFB1309604) and National Natural Science of Foundation of China (grant no. 51875281, 51861135306).

This study was carried out in accordance with the Guide for Laboratory Animal Management Ordinance of China. The experimental procedures were approved by the Jiangsu Association for Animal Science (Jiangsu, China).

* All supplementary materials are available at https://doi.org/10.1007/s42235-021-0061-8.

References

[1] Dickinson M H, Lehmann F O, Sane S P. Wing rotation and the aerodynamic basis of insect flight. *Science*, 1999, **284**, 1954–1960.

[2] Walker S M, Thomas A L R, Taylor G K. Deformable wing kinematics in free-flying hoverflies. *Journal of the Royal Society Interface*, 2010, **7**, 131–142.

[3] Sun M, Xiong Y. Dynamic flight stability of a hovering bumblebee. *Journal of Experimental Biology*, 2005, **208**, 447–459.

[4] Bomphrey R J, Lawson N J, Taylor G K, Thomas A L R. Application of digital particle image velocimetry to insect aerodynamics: Measurement of the leading-edge vortex and

near wake of a Hawkmoth. *Experiments in Fluids*, 2006, **40**, 546–554.

[5] Zanker J M. The wing beat of drosophila melanogaster. III Control. *Philosophical Transactions of the Royal Society of London Biological Sciences*, 1990, **327**, 45–64.

[6] Karl G G, Bärbel H, Biesinger R. Optomotor control of wing beat and body posture in Drosophila. *Biological Cybernetics*, 1979, **35**, 101–112.

[7] David C T. 1985 Visual control of the partition of flight force between lift and thrust in free-flying Drosophila. *Nature*, **313**, 48–50.

[8] Au L T K, Phan V H, Park H C. Longitudinal flight dynamic analysis on vertical takeoff of a tailless flapping-wing micro air vehicle. *Journal of Bionic Engineering*, 2018, **15**, 283–297.

[9] Pond C M. The initiation of flight in unrestrained locusts, Schistocerca. *Journal of Comparative Physiology B-Biochemical Systems and Environmental Physiology*, 1972, **802**, 163–178.

[10] Burrows M, Morris O. Jumping and kicking in bush crickets. *Journal of Experimental Biology*, 2003, **206**, 1035–1049.

[11] Card G, Dickinson M H. Performance trade-offs in the flight initiation of drosophila. *Journal of Experimental Biology*, 2008, **211**, 341–353.

[12] Burrows M. Kinematics of jumping in leafhopper insects (Hemiptera, Auchenorrhyncha, Cicadellidae). *Journal of Experimental Biology*, 2007, **210**, 3579–3589.

[13] Crandell K E, Tobalske B W. Kinematics and aerodynamics of avian upstrokes during slow flight. *Journal of Experimental Biology*, 2015, **218**, 2518–2527.

[14] Tobalske B W, Altshuler D L, Powers D R. Take-off mechanics in hummingbirds (Trochilidae). *Journal of Experimental Biology*, 2004, **207**, 1345–1352.

[15] Fontaine E I, Zabala F, Dickinson M H, Burdick J W. Wing and body motion during flight initiation in drosophila revealed by automated visual tracking. *Journal of Experimental Biology*, 2009, **212**, 1307–1323.

[16] Xu N, Sun M. Lateral dynamic flight stability of a model bumblebee in hovering and forward flight. *Journal of Theoretical Biology*, 2013, **319**, 102–115.

[17] Truong T, Le T, Park H, Yoon K, Kim M, Byun D. Non-jumping take off performance in beetle flight (Rhinoceros Beetle Trypoxylus dichotomus. *Journal of Bionic Engineering*, 2014, **11**, 61–71.

[18] Sunada S, Kawachi K, Watanabe I. Performance of a butterfly in take-off flight. *Journal of Experimental Biology*, 1993, **183**, 249–277.

[19] Burrows M. Jumping mechanisms of treehopper insects (Hemiptera, Auchenorrhyncha, Membracidae). *Journal of Experimental Biology*, 2013, **216**, 788–799.

[20] Theriault D H, Fuller N W, Jackson B E, Bluhm E, Evangelista D, Wu Z, Betke M, Hedrick T L. A protocol and calibration method for accurate multi-camera field videography. *Journal of Experimental Biology*, 2014, **217**, 1843–1848.

[21] Hedrick T L. Software techniques for two- and three-dimensional kinematic measurements of biological and biomimetic systems. *Bioinspiration & Biomimetics*, 2008, **3**, 34001.

[22] Hikaru A, Liang F Y, Liu H. Near- and far-field aerodynamics in insect hovering flight: an integrated computational study. *Journal of Experimental Biology*, 2008, **211**, 239–257.

[23] Poelma C, Dickson W B, Dickinson M H. Time-resolved reconstruction of the full velocity field around a dynamically-scaled flapping wing. *Experiments in Fluids*, 2006, **41**, 213–225.

[24] Bimbard G, Kolomenskiy D, Bouteleux O, Casas J, Godoy-Diana R. Force balance in the take-off of a pierid butterfly: Relative importance and timing of leg impulsion and aerodynamic forces. *Journal of Experimental Biology*, 2013, **216**, 3551–3563.

[25] Ramamurti R, Sandberg W C. A computational investigation of the three-dimensional unsteady aerodynamics of Drosophila hovering and maneuvering. *Journal of Experimental Biology*, 2007, **210**, 881–896.

[26] Burrows M, Ghosh A, Yeshwanth H M, Dorosenko M, Sane S P. Effectiveness and efficiency of two distinct mechanisms for take-off in a derbid planthopper insect. *Journal of Experimental Biology*, 2019, **222**, 1–12.

[27] Berg A M, Biewener A A. Wing and body kinematics of takeoff and landing flight in the pigeon (Columba livia). *Journal of Experimental Biology*, 2010, **213**, 1651–1658.

[28] Burrows M. Biomechanics: Froghopper insects leap to new heights. *Nature*, 2003, **424**, 509.

[29] Provini P, Tobalske B W, Crandell K E, Abourachid A. Transition from leg to wing forces during take-off in birds. *Journal of Experimental Biology*, 2012, **215**, 4115–4124.

[30] Wang H, Zeng L, Liu H, Yin C. Measuring wing kinematics, flight trajectory and body attitude during forward flight and turning maneuvers in dragonflies. *Journal of Experimental Biology*, 2003, **206**, 745–757.

[31] Fry S N, Sayaman R, Dickinson M H. The aerodynamics of free-flight maneuvers in drosophila. *Science*, 2003, **300**, 495–498.

[32] Akira A, Tadaaki W. Flight performance of a dragonfly. *Journal of Experimental Biology*, 1988, **137**, 221–252.

[33] Li X, Guo C. Wing-kinematics measurement and flight modelling of the bamboo weevil *C. buqueti*. *IET Nanobiotechnology*, 2020, **14**, 53–58.

[34] Alexander D E. Wind tunnel studies of turns by flying dragonflies. *Journal of Experimental Biology*, 1986, **122**, 81–98.

[35] Chen M W, Zhang Y L, Sun M. Wing and body motion and aerodynamic and leg forces during take-off in droneflies. *Journal of the Royal Society Interface*, 2013, **10**, 20130808.

[36] Ellington C P, Berg C, Willmott A P, Thomas A. Leading-edge vortices in insect flight. *Nature*, 1996, **384**, 626–630.

[37] van den Berg C, Ellington C P. The three–dimensional leading–edge vortex of a 'hovering' model hawkmoth. *Philosophical Transactions of the Royal Society B*: *Biological Sciences*, 1997, **352**, 329–340.

[38] Liu H, Ellington C P, Kawachi K A. A computational fluid dynamic study of hawkmoth hovering. *Journal of Experimental Biology*, 1998, **201**, 461–477.

[39] Liu H and Kawachi K. A numerical study of insect flight. *Journal of Computational Physics*, 1998, **146**, 124–156.

[40] Aono H, Liu H. Vortical structure and aerodynamics of hawkmoth hovering. *Journal of Biomechanical Science & Engineering*, 2006, **1**, 234–245.

[41] Warrick D R, Tobalske B W, Powers D R. Aerodynamics of the hovering hummingbird. *Nature*, 2005, **435**, 1094–1097.